Collapse and revival of quantum many-body scars via Floquet engineering

Bhaskar Mukherjee,[1] Sourav Nandy,[1] Arnab Sen,[1] Diptiman Sen,[2] and K. Sengupta[1]
[1]*School of Physical Sciences, Indian Association for the Cultivation of Science, Kolkata 700032, India*
[2]*Centre for High Energy Physics and Department of Physics, Indian Institute of Science, Bengaluru 560012, India*

(Received 17 January 2020; revised manuscript received 17 May 2020; accepted 20 May 2020; published 1 June 2020)

The presence of quantum scars, athermal eigenstates of a many-body Hamiltonian with finite-energy density, leads to an absence of ergodicity and long-time coherent dynamics starting from initial states that have a high overlap with scars as experimentally observed in a chain of ultracold Rydberg atoms. We show, via study of a periodically driven Rydberg chain, that the drive frequency acts as a tuning parameter for several reentrant transitions between ergodic and weak ergodicity breaking regimes. The former regime shows rapid thermalization of correlation functions and absence of scars in the Floquet spectrum of the system. The latter regime, in contrast, has scars; they lead to long-time coherent dynamics of correlation functions. We provide an analytical explanation of the existence of these regimes by going beyond a high-frequency Magnus expansion and using a novel perturbative approach valid at large drive amplitudes to derive a Floquet Hamiltonian which qualitatively explains the behavior of the driven system at *arbitrary* frequencies. We also discuss experiments involving finite Rydberg chains which can validate our theory. Our results demonstrate the possibility of drive-frequency-induced tuning between ergodic and weak ergodicity breaking dynamics in a disorder-free quantum many-body system.

DOI: 10.1103/PhysRevB.101.245107

I. INTRODUCTION

The eigenstate thermalization hypothesis (ETH) is one of the central paradigms for understanding out-of-equilibrium dynamics of closed nonintegrable quantum systems [1–8]. It posits that *all* bulk eigenstates of a generic quantum many-body Hamiltonian are thermal; their presence ensures ergodicity and leads to eventual thermalization for out-of-equilibrium dynamics of a generic many-body state [5]. This hypothesis is strongly violated in certain cases, the most famous example being one-dimensional (1D) disordered electrons in their many-body localized phase [9,10]. More recently another example of a weaker failure of ETH, due to the presence of quantum many-body scar states, has been studied extensively in disorder-free systems [11–22]. Scars are eigenstates with finite-energy density but anomalously low entanglement [12,14–16,19] which form an almost closed subspace in the system's Hilbert space under the action of its Hamiltonian. Their presence leads to persistent coherent oscillatory dynamics of correlation functions starting from initial states that have a high overlap with scars. This provides an observable consequence of their presence as verified in recent experiments on quench dynamics of a chain of ultracold Rydberg atoms [12].

In this work, we study the fate of such ergodicity violation in a periodically driven Rydberg chain described by its Floquet Hamiltonian H_F [23]. H_F is related to the system's unitary evolution operator U: $U(T,0) = \exp[-iH_F T/\hbar]$, where $T = 2\pi/\omega_D$ is the drive time period and ω_D is the drive frequency. For generic disorder-free systems, such driving is expected to cause thermalization to a featureless "infinite temperature" state [24–27]. In what follows, we will study the possibility of the existence of scar states in the eigenstates of H_F as a function of ω_D and relate their influence on the dynamics of correlation functions. Our initial state will be an experimentally realized $\mathbb{Z}_2$ symmetry broken many-body state which has one Rydberg excitation on alternate lattice sites [12,28–30].

The central results of this study are as follows. Starting from an initial $\mathbb{Z}_2$ state, we unravel several drive-frequency-induced transitions between two distinct dynamical regimes. In the weak ergodicity breaking (coherent) regime, long-time persistent oscillations of the density-density correlators of Rydberg atoms survive and have characteristic frequencies which are different from ω_D indicating a lack of synchronization (a hallmark of thermalization in periodically driven systems). In contrast, in the ergodic (thermal) regime, we find that the behavior of the correlators agrees with that expected from ETH. These transitions provide a route to controlled switching between ergodic and weak ergodicity breaking dynamics of the Rydberg atoms. Furthermore, in the coherent regime, the oscillation frequency of the correlators can be controlled by tuning ω_D. We relate these features, which have no analogs in nondriven systems studied earlier [12–22], to the presence or absence of quantum scars in the eigenspectrum of H_F and discuss experiments which can test our theory. We also use a novel perturbation theory in the large drive amplitude regime to derive a Floquet Hamiltonian for the system which explains this behavior and provides a qualitative understanding of the propertes of the driven system at both high and low frequencies. We show that this Floquet Hamiltonian reproduces its counterpart obtained by a standard Magnus expansion in the high-frequency regime and constitutes an exact resummation of it to all orders in the limit of high drive amplitude.

The rest of the paper is organized as follows. In Sec. II, we introduce the model which we use for our computation and derive the Floquet Hamiltonian of the system. This is followed by Sec. III, where we present out numerical result and interpret them using the Floquet Hamiltonian. Finally, in Sec. IV, we summarize our results, discuss experiments which can test them, and conclude. Further details of our calculations are presented in Appendices A and B.

II. MODEL AND FLOQUET HAMILTONIAN

In this section, we first introduce the model Hamiltonian which shall be the starting point of our analysis in Sec. II A. This is followed by the derivation of the Floquet Hamiltonian using Magnus expansion in Sec. II B. Finally in Sec. II C, we introduce the perturbation theory valid for large drive amplitudes and derive a Floquet Hamiltonian from it which reproduces its Magnus counterpart in the high-frequency limit and qualitatively explains the properties of the driven system at arbitrary frequencies.

A. Model Hamiltonian

The Hamiltonian of the Bose-Hubbard model with a tilt is given by [31,32]

$$H = -w' \sum_{\langle ij \rangle} (b_i^\dagger b_j + \text{H.c.}) - \sum_i (\mu + E_0 i) n_i^b + \sum_i \frac{U}{2} n_i^b (n_i^b - 1), \tag{1}$$

where b_i ($b_i^\dagger$) denotes the boson annihilation (creation) operator on site i of a 1D chain, $n_i^b = b_i^\dagger b_i$ is the boson number operator, w' is the hopping amplitude of the bosons, E_0 denotes the magnitude of the tilt, μ is the chemical potential, w is the hopping amplitude, and U is the on-site interaction between the bosons. The tilt can be generated either by shifting the center of the parabolic trap confining the bosons or by applying a linearly varying Zeeman field which couples to the spin of the bosons. The latter variation can be made time dependent by using a magnetic field which varies periodically in time. It is well known that the low-energy physics of these bosons deep inside the Mott phase, whose occupation number is denoted by n_0 (here we focus on the case $n_0 = 1$) and where $U, E_0 \gg w'$, $|U - E_0|$ is given by

$$H_d = -w \sum_\ell (d_\ell + d_\ell^\dagger) + \lambda \sum_\ell n_\ell, \tag{2}$$

where $d_\ell = b_i^\dagger b_j / \sqrt{n_0(n_0+1)}$ denotes a dipole annihilation operator on link ℓ between sites neighboring i and j on a 1D lattice, $w = \sqrt{2} w'$ for $n_0 = 1$, $n_\ell = d_\ell^\dagger d_\ell$ is the dipole number operator on link ℓ, w is the amplitude of spontaneous dipole creation or destruction, and λ is the chemical potential for the dipoles. This dipole model is to be supplemented by two constraints which make it nonintegrable: $n_\ell \leqslant 1$ and $n_\ell n_{\ell+1} = 0$ for all links. The phase diagram of this model has been studied theoretically in Ref. [31] and has also been experimentally verified [33]. It is well-known that H_d supports a quantum phase transition at $\lambda_c = -1.31w$ separating a $\mathbb{Z}_2$ symmetry broken ground state ($|\mathbb{Z}_2\rangle$) for $\lambda < \lambda_c$ and a featureless dipole vacuum ($|0\rangle$) for $\lambda > \lambda_c$. The nonequilibrium dynamics of this model has also been studied for quench, ramp, and periodic protocols [34].

The dipole model described in Eq. (2) also serves as an effective model for describing the low energy physics of the Rydberg atoms. To see this we first consider the Hamiltonian of such atoms given by [12–22,28–30]

$$H_{\text{RYD}} = \sum_i \left(\Omega \sigma_i^x + \Delta n_i^r\right) + \sum_{ij} V_{ij} n_i^r n_j^r. \tag{3}$$

Here $n_i^r \leqslant 1$ denotes the number of Rydberg excitations on a given site, Δ is the detuning parameter which can be used to excite an atom to its Rydberg state, V_{ij} denotes the interaction between two Rydberg excitations, $\sigma_i^x = |g_i\rangle\langle r_i|$ denotes the coupling between the ground ($|g\rangle$) and Rydberg excited ($|r\rangle$) states, and Ω is the corresponding coupling strength. In experiments [12], it is possible to reach a regime where $V_{i,i+1} \gg \Omega, \Delta \gg V_{i,i+2}$; in this case, the Hamiltonian model becomes equivalent to that of

$$H'_{\text{RYD}} = \sum_i \left(\Omega \sigma_i^x + \Delta n_i^r\right), \tag{4}$$

supplemented by the constraint that $n_i^r n_{i+1}^r = 0$ for all sites i. Clearly, this model is equivalent to Eq. (2) with the identification $n_i^r \to n_\ell$, $\Delta \to \lambda$, and $\Omega \to -w$.

Furthermore it is also easy to see that the dipole Hamiltonian [Eq. (2)] is identical to the PXP model studied in Ref. [12] for $\lambda = 0$. The simplest way to see this involves mapping of the dipole operators to Ising spins via the transformation

$$\sigma_\ell^z = 2n_\ell - 1, \quad \sigma_\ell^{x(y)} = (i)\,(d_\ell + (-) d_\ell^\dagger), \tag{5}$$

where σ^α denote the Pauli matrices for $\alpha = x, y, z$. Moreover, the constraint of not having dipoles on adjacent links can be implemented via a local projection operator $P_\ell = (1 - \sigma_\ell^z)/2$ [12–22]. Using these, one finds the spin Hamiltonian

$$H_{\text{spin}} = -w \sum_\ell P_{\ell-1} \sigma_\ell^x P_{\ell+1} + \frac{\lambda}{2} \sum_\ell \sigma_\ell^z = \sum_\ell \left(-w \tilde{\sigma}_\ell^x + \frac{\lambda}{2} \sigma_\ell^z\right), \tag{6}$$

where $\tilde{\sigma}_\ell^\alpha = P_{\ell-1} \sigma_\ell^\alpha P_{\ell+1}$ for $\alpha = x, y, z$, and we have ignored an unimportant constant term while writing down the expression for H_{spin}. The physics of H_{spin} within the constrained dipole Hilbert space is identical to that of H_d and H_{RYD}. At $\lambda = 0$, H_{spin} reduced to the PXP model studied in Ref. [12]. Note that both the constraints of the dipole model are incorporated in H_{spin} via the local projection operators P_ℓ.

Equation (6) shall be used for all analysis in the rest of this work.

B. Magnus expansion

We consider the Hamiltonian H_{spin} given by Eq. (6) in the presence of a periodic drive characterized by a square pulse protocol with time period $T = 2\pi/\omega_D$, where ω_D is the drive frequency: $\lambda(T) = -(+)\lambda$ for $t \leqslant (>) T/2$. In what follows, we will chart out the details of the computation of the Floquet Hamiltonian of such a driven system using a high-frequency Magnus expansion.

For this protocol, the unitary matrix governing the evolution by a time period is given by

$$U = e^{-iH_+T/(2\hbar)}e^{-iH_-T/(2\hbar)} = e^{X_+}e^{X_-} = U_+U_-, \tag{7}$$

where $X_\pm = (-iT/2\hbar)H_\pm$. For future reference, we also define $X_{1,2}$ given by

$$X_{1[2]} = \left(\frac{i\hbar}{2T}\right) w\left[-\frac{\lambda}{2}\right] \sum_\ell \tilde{\sigma}^x_\ell [\sigma^z_\ell], \tag{8}$$

such that $X_\pm = X_1 \pm X_2$. The Floquet Hamiltonian can be obtained from U as $H_F = (i\hbar/T)\ln U$. Using the Baker-Campbell-Hausdorff formula, one can express

$$\begin{aligned}\ln[e^{X_+}e^{X_-}] = X_+ + X_- + \frac{1}{2}[X_+, X_-] \\ + \frac{1}{12}[X_+ - X_-, [X_+, X_-]] \\ - \frac{1}{24}[X_-, [X_+, [X_+, X_-]]] + \cdots .\end{aligned} \tag{9}$$

From Eq. (9) we can find terms of different order in the Floquet Hamiltonian. The computation of these terms up to $O(1/\omega_D^2)$ is straightforward and yields

$$\begin{aligned} H^0_F &= -w\sum_\ell \tilde{\sigma}^x_\ell, \quad H^1_F = -w\gamma \sum_\ell \tilde{\sigma}^y_\ell, \\ H^2_F &= \frac{2w}{3}\gamma^2 \sum_\ell \tilde{\sigma}^x_\ell, \end{aligned} \tag{10}$$

where $\gamma = \lambda T/(4\hbar)$. Note that these terms lead to a renormalized PXP model; it amounts to a change of magnitude of the coefficient w of the standard PXP Hamiltonian and also a rotation in spin-space which depends on ω_D. Note that the second-order term in the expansion has an opposite sign compared to the zeroth-order term. As we will see later, this is a general feature of the model; any term $\sim\gamma^n$ in the renormalized PXP model always comes with a opposite sign compared to a term $\sim\gamma^{n-2}$.

The first nontrivial longer-ranged terms in H_F arises in $\mathcal{O}(1/\omega_D^3)$. Its derivation involves some subtle issues. To see this, let us consider the commutator $C_1 = [X_+, [X_+, X_-]] = C_{1a} + C_{1b}$. It is easy to see after a straightforward calculation that

$$\begin{aligned} C_{1a} &= -2w\lambda^2\left(\frac{iT}{2\hbar}\right)^3 \sum_\ell \tilde{\sigma}^x_\ell, \\ C_{1b} &= -2w^2\lambda\left(\frac{iT}{2\hbar}\right)^3 \sum_\ell \big[P_{\ell-2}\sigma^x_{\ell-1}\sigma^x_\ell P_\ell P_{\ell+1} \\ &\quad + P_{\ell-2}P_{\ell_1}\sigma^y_{\ell-1}\sigma^y_\ell P_{\ell+1} + 2\tilde{\sigma}^\ell_z \\ &\quad + P_{\ell-1}\sigma^x_\ell P_\ell \sigma^x_{\ell+1}P_{\ell+2} + P_{\ell-1}\sigma^y_{\ell-1}P_\ell\sigma^x_{\ell+1}P_{\ell+2}\big]. \end{aligned} \tag{11}$$

We note that within the constrained Hilbert space, any term with $\sigma^\alpha_{\ell-1}\sigma^\beta_\ell P_\ell$ identically vanishes for $\alpha, \beta = x, y$. Furthermore, the projection operators P_ℓ on any link satisfy $(1 - P_{\ell\pm1})\sigma^\alpha_\ell = 0$ for $\alpha = x, y$. Using these results, we can simplify C_{1b} to obtain

$$C_{1b} = -2w^2\lambda\left(\frac{iT}{2\hbar}\right)^3 \sum_\ell \left(2\tilde{\sigma}^\ell_z + \tilde{\sigma}^\ell_x\tilde{\sigma}^\ell_x + \tilde{\sigma}^\ell_y\tilde{\sigma}^\ell_y\right). \tag{12}$$

Using Eq. (12) and evaluating the necessary commutators, we finally get $H^{(3)}_F = H^{(1)}_{F3} + H^{(2)}_{F3} + H^{(3)}_{F3}$, where

$$H^{(1)}_{F3} = \frac{w\gamma^3}{3}\sum_\ell \tilde{\sigma}^y_\ell, \tag{13}$$

$$H^{(2)}_{F3} = \frac{4\lambda\delta^3}{3}\sum_\ell \left[\tilde{\sigma}^y_{\ell-1}\tilde{\sigma}^z_\ell + \tilde{\sigma}^z_\ell\tilde{\sigma}^y_{\ell+1}\right], \tag{14}$$

$$H^{(3)}_{F3} = \frac{2\lambda\delta^3}{3}\sum_\ell \left(\tilde{\sigma}^y_\ell\sigma^z_{\ell+1}P_{\ell+2} + P_{\ell-2}\sigma^z_{\ell-1}\tilde{\sigma}^y_\ell\right). \tag{15}$$

Here $\delta = wT/(4\hbar)$, and we note that all adjacent two spin terms such as $\tilde{\sigma}^y_j\tilde{\sigma}^x_{j\pm1}$ and three spin terms such as $\tilde{\sigma}^y_j\tilde{\sigma}^y_{j+1}\tilde{\sigma}^y_{j+2}$ vanish within the constrained Hilbert space. Eqs. (10), (13), (14), and (15) yield the final Magnus Floquet Hamiltonian.

Before ending this section we note that if we concentrate on the large λ/w limit, it is possible to compute higher-order corrections to the coefficients in H^0_F and H^1_F. This can be seen by noting that at each order the contribution to such terms comes from $[X_2, [X_2, [X_2, \cdots [X_2, X_1]]]\cdots]$, i.e., the nth-order contribution involves commutator of $n-1$ terms involving σ^z_j and one $\tilde{\sigma}^x_j$. These commutators provide the leading contribution in the large λ/w limit. This structure allows us to compute leading higher-order terms in the Magnus expansion which contribute to the coefficients of the PXP term. A straightforward but cumbersome computation yields

$$\begin{aligned} H_2 = -w\Bigg(&\left[1 - \frac{2\gamma^2}{3} + \frac{2\gamma^4}{15} - \frac{4\gamma^6}{315} + \frac{2\gamma^8}{2835} - \frac{4\gamma^{10}}{155925} + \cdots\right]\sum_l \tilde{\sigma}^x_l \\ &+\gamma\left[1 - \frac{\gamma^2}{3} + \frac{2\gamma^4}{45} - \frac{\gamma^6}{315} + \frac{2\gamma^8}{14175} - \frac{2\gamma^{10}}{467775} + \cdots\right]\sum_l \tilde{\sigma}^y_l\Bigg). \end{aligned} \tag{16}$$

It will be shown in Sec. II C that the coefficients in H_2 can be resummed to yield a closed form valid for arbitrary ω_D: $H_F = -[(w\sin\gamma)/\gamma]\sum_j(\cos\gamma\tilde{\sigma}^x_j + \sin\gamma\tilde{\sigma}^y_j)$. Note that such a resummation is possible only in the limit $w/|\lambda| \ll 1$.

C. Floquet perturbation theory

We will now present a perturbation theory for a periodically driven system [35] that allows us to go to arbitrary drive frequencies in the limit of large drive amplitude. We consider a Hamiltonian $H(t) = H_0(t) + V$, where $H_0(t)$ varies in time with a period $T = 2\pi/\omega$, and V is a small time-independent perturbation. We will assume that $H_0(t)$ commutes with itself at different times, and will work in the basis of eigenstates of $H_0(t)$ which are time-independent and will be denoted as $|n\rangle$, so that $H_0(t)|n\rangle = E_n(t)|n\rangle$, and $\langle m|n\rangle = \delta_{mn}$. We will also assume that V is completely off-diagonal in this basis, namely, $\langle n|V|n\rangle = 0$ for all n. We will now find solutions of the Schrödinger equation

$$i\hbar \frac{\partial |n(t)\rangle}{\partial t} = H(t)|n(t)\rangle, \tag{17}$$

which satisfy

$$|n(T)\rangle = e^{-i\theta_n}|n(0)\rangle. \tag{18}$$

For $V = 0$, we have $|n(t)\rangle = e^{-(i/\hbar)\int_0^t dt' E_n(t')}|n\rangle$, so that the eigenvalue of the Floquet operator U is given by

$$e^{-i\theta_n} = e^{-(i/\hbar)\int_0^T dt E_n(t)}. \tag{19}$$

We will now develop a perturbation theory to first order in V. We assume that the nth eigenstate can be written as

$$|n(t)\rangle = \sum_m c_m(t) e^{-(i/\hbar)\int_0^t dt' E_m(t')}|m\rangle, \tag{20}$$

where $c_n(t) \simeq 1$ for all t, while $c_m(t)$ is of order V for all $m \neq n$ and all t. Equation (17) implies that

$$\begin{aligned} i\hbar \sum_m \dot{c}_m(t) e^{-(i/\hbar)\int_0^t dt' E_m(t')}|m\rangle \\ = V \sum_m c_m(t)\, e^{-(i/\hbar)\int_0^t dt' E_m(t')}|m\rangle, \end{aligned} \tag{21}$$

where the dot over c_m denotes d/dt. Taking the inner product of Eq. (21) with $\langle n|$ and using $\langle n|V|n\rangle = 0$, we find that $\dot{c}_n = 0$. We can therefore choose $c_n(t) = 1$ for all t. We thus have

$$\begin{aligned} |n(t)\rangle = e^{-i\int_0^t dt' E_n(t')}|n\rangle \\ + \sum_{m\neq n} c_m(t)\, e^{-i\int_0^t dt' E_m(t')}|m\rangle. \end{aligned} \tag{22}$$

Hence, Eq. (18) implies that the Floquet eigenvalue is still given by Eq. (19) up to first order in V.

Next, taking the inner product of Eq. (21) with $\langle m|$, where $m \neq n$, and integrating from $t = 0$ to T, we get

$$c_m(T) = c_m(0) - \frac{i}{\hbar}\langle m|V|n\rangle \int_0^T dt e^{i\int_0^t dt'[E_m(t') - E_n(t')]}. \tag{23}$$

Since we know that Eq. (22) satisfies

$$|n(T)\rangle = e^{-(i/\hbar)\int_0^T dt E_n(t)}|n(0)\rangle, \tag{24}$$

we must have

$$c_m(T) = e^{(i/\hbar)\int_0^T dt[E_m(t) - E_n(t)]} c_m(0) \tag{25}$$

for all $m \neq n$. Eqs. (23)–(25) imply that we must choose

$$c_m(0) = -\frac{i}{\hbar}\langle m|V|n\rangle \frac{\int_0^T dt e^{(i/\hbar)\int_0^t dt'[E_m(t') - E_n(t')]}}{e^{(i/\hbar)\int_0^T dt[E_m(t) - E_n(t)]} - 1}. \tag{26}$$

We see that $c_m(t)$ is indeed of order V provided that the denominator on the right-hand side of Eq. (26) does not vanish; we will call this case nondegenerate.

The above analysis breaks down if

$$e^{(i/\hbar)\int_0^T dt[E_m(t) - E_n(t)]} = 1, \tag{27}$$

for a pair of states $|m\rangle$ and $|n\rangle$. We then have to develop a degenerate perturbation theory. Suppose that there are p states $|m\rangle$ ($m = 1, 2, \cdots, p$) which have energy eigenvalues $E_m(t)$ satisfying Eq. (27) for every pair of states. Ignoring all the other states of the system for the moment, we will assume that a solution of the Schrödinger equation is given by

$$|\psi(t)\rangle = \sum_{m=1}^{p} c_m(t) e^{-(i/\hbar)\int_0^t dt' E_m(t')}|m\rangle, \tag{28}$$

where we now allow all the $c_m(t)$'s to be order 1. Then we again obtain an equation like Eq. (21) except that the sum over m only goes over p states. To first order in V, we can replace $c_m(t)$ by the time-independent constants $c_m(0)$ on the right-hand side of Eq. (21). Upon integrating from $t = 0$ to T, this gives

$$\begin{aligned} c_m(T) = c_m(0) - \frac{i}{\hbar}\sum_{n=1}^{p}\langle m|V|n\rangle \\ \times \int_0^T dt e^{(i/\hbar)\int_0^t dt'[E_m(t') - E_n(t')]} c_n(0). \end{aligned} \tag{29}$$

This can be written as a matrix equation

$$c(T) = [I - iM]c(0), \tag{30}$$

where $c(t)$ denotes the column $[c_1(t), c_2(t), \cdots, c_p(t)]^T$ (where the superscript T denotes transpose), I is the p-dimensional identity matrix, and M is a p-dimensional Hermitian matrix with matrix elements given by

$$M_{mn} = \frac{\langle m|V|n\rangle}{\hbar}\int_0^T dt e^{(i/\hbar)\int_0^t dt'[E_m(t') - E_n(t')]}. \tag{31}$$

Let the eigenvalues of M be given by μ_n ($n = 1, 2, \cdots, p$). To first order in V, $I - iM$ is a unitary matrix and will therefore have eigenvalues of the form $e^{-i\mu_n}$; the corresponding eigenstates satisfy $c(T) = e^{-i\mu_n}c(0)$. Next, we want the wave function in Eq. (28) to satisfy $|\psi(T)\rangle = e^{-i\theta_n}|\psi(0)\rangle$. This implies that the Floquet eigenvalues are related to the eigenvalues of M as

$$e^{-i\theta_n} = e^{-i\mu_n - (i/\hbar)\int_0^T dt E_n(t)}. \tag{32}$$

Given a Floquet operator U, we can define a Floquet Hamiltonian H_F as $U = e^{-iH_F T/\hbar}$. Comparing this with Eqs. (30) and (31), we see that the matrix elements of H_F are

given by

$$(H_F)_{mn} = \frac{M_{mn}}{T} = \frac{\langle m|V|n\rangle}{T}\int_0^T dt\, e^{(i/\hbar)\int_0^t dt'[E_m(t')-E_n(t')]}. \quad (33)$$

We will now apply the above analysis to our model, where

$$H_0(t) = \frac{\lambda(t)}{2}\sum_l \sigma_l^z,$$
$$V = -w\sum_l P_{l-1}\sigma_l^x P_{l+1}, \quad (34)$$

with $\lambda(t) = -\lambda$ for $0 < t < T/2$ and $+\lambda$ for $T/2 < t < T$. We will do Floquet perturbation theory assuming that $w \ll \lambda$. To do this, we consider states in the σ_l^z basis. According to the Hamiltonian $H_0(t)$ in Eq. (34), all such states $|n\rangle$ have an instantaneous energy eigenvalue $E_n(t) = (\lambda(t)/2)\sum_l \sigma_l^z$, which implies that the $\int_0^T dt E_n(t) = 0$. Thus, the unperturbed Floquet eigenvalue $e^{-i\theta_n}$ is equal to 1 for all states; we therefore have to do degenerate perturbation theory.

If $|m\rangle$ and $|n\rangle$ are two states which are connected by the perturbation V in Eq. (34), then they differ by the value of σ_l^z at only one site and therefore $E_m(t) - E_n(t) = \lambda(t)$, assuming that $|m\rangle$ and $|n\rangle$ have spin-up and spin-down respectively at that site. We find that the integral in Eq. (29) is given by

$$\int_0^T dt e^{(i/\hbar)\int_0^t dt'[E_m(t')-E_n(t')]} = \frac{i2}{\lambda}(e^{-i\lambda T/2\hbar} - 1). \quad (35)$$

We therefore see that if

$$\frac{\lambda}{\hbar\omega} = 2q, \quad (36)$$

where q is an integer, then the expression in Eq. (35) vanishes. This means that even in degenerate perturbation theory, there is no change in the Floquet eigenvalues and they remain equal to 1.

We will now use Eqs. (33) and (35). If $|m\rangle$ and $|n\rangle$ are two states which are connected by the perturbation V, then we have $\langle m|V|n\rangle = -w$. We then obtain

$$(H_F)_{mn} = -\frac{i2\hbar w}{\lambda T}(e^{-i\lambda T/2\hbar} - 1) = -\frac{w}{\gamma}e^{-i\gamma}\sin\gamma, \quad (37)$$

where $\gamma = \pi\lambda/(2\hbar\omega)$. To $\mathcal{O}(w)$, the Floquet Hamiltonian is therefore given by

$$H_F^{(1)} = -w\frac{\sin\gamma}{\gamma}\sum_n\left[\cos\gamma\tilde{\sigma}_n^x + \sin\gamma\tilde{\sigma}_n^y\right]. \quad (38)$$

This vanishes if Eq. (36) is satisfied; we will then have to go to higher order in perturbation theory. A unitary rotation by an angle of $-\gamma$ with respect to the z axis in spin space converts Eq. (38) into an effective PXP Hamiltonian and hence we refer to $H_F^{(1)}$ as PXP terms. Longer-ranged non-PXP terms are progressively generated at higher orders in the perturbation theory for the Floquet Hamiltonian. The local constraints of the Hilbert space and the symmetric form of $\lambda(t)$ fixes the form of the lowest-order non-PXP term in the Floquet Hamiltonian to be

$$H_F^{(2)} = \left(C\sum_n \tilde{\sigma}_{n-1}^+\tilde{\sigma}_{n+1}^+\tilde{\sigma}_n^- + \text{H.c.}\right) + \cdots, \quad (39)$$

where $C = \mathcal{O}(w^3/\lambda^3)$ and the ellipses denote terms that are higher order in w/λ. The analytic form of C requires a more detailed calculation which is left for future work.

We note that Eq. (38) can also be obtained by a straightforward expansion of the evolution operators $U_\pm$ [36]. To see this, we first note that for any two different sites j and j' we have

$$\left[-w\tilde{\sigma}_j^x \pm \frac{\lambda}{2}\sigma_j^z, -w\tilde{\sigma}_{j'}^x \pm \frac{\lambda}{2}\sigma_{j'}^z\right] \sim \mathcal{O}(w^2). \quad (40)$$

Thus, as long as we are interested in terms of $\mathcal{O}(w)$, we can write

$$U_\pm \simeq \prod_j e^{-iT(-w\tilde{\sigma}_j^x \pm \frac{\lambda}{2}\sigma_j^z)/2\hbar}. \quad (41)$$

One can then carry out a straightforward expansion of $U_\pm$. A few lines of algebra, required to gather terms of $\mathcal{O}(w/\lambda)$, yield

$$U_\pm \simeq \prod_j\left[\cos(\gamma) \mp i\sigma_z^j\sin(\gamma) - i\frac{2w}{\lambda}\sin(\gamma)\tilde{\sigma}_j^x\right]. \quad (42)$$

Using Eq. (42), one can compute $U = U_+U_-$. A re-exponentiation of terms of $\mathcal{O}(w/\lambda)$ then yields Eq. (38) in a straightforward manner.

In the next section, we shall use Eq. (38) and the competition between the PXP [Eq. (38)] and the non-PXP terms [Eq. (39)] in the Floquet Hamiltonian to obtain a qualitative understanding of our results. Here we note that Eq. (38) can also be obtained by summing the leading terms in λ to all orders ω_D in the Magnus expansion. Stated differently, the $\lambda \gg w$ limit allows for Floquet engineering of H_F at *arbitrary* ω_D where w/λ acts as the control parameter. We also note that the norm of $H_F^{(1)}$ [Eq. (38)] vanishes at $\gamma = n_0\pi$ or $\lambda/(\hbar\omega_D) = 2n_0$ for nonzero integers n_0 allowing the non-PXP terms in $H_F^{(2)}$ to compete with PXP terms in $H_F^{(1)}$ in the vicinity of such drive frequencies; this feature will be used to understand the transitions between ergodic and weak ergodicity breaking regimes.

III. NUMERICAL RESULTS

In this section, we provide numerical analysis of the driven system. To this end, we note that the unitary evolution operator at the end of a drive cycle is given by

$$U(T,0) = e^{-iH_{\text{spin}}[\lambda]T/2}e^{-iH_{\text{spin}}[-\lambda]T/2}. \quad (43)$$

The evolution operator can then be expressed as

$$U(T,0) = \sum_{p,q} e^{-i(\epsilon_q^+ + \epsilon_p^-)T/2}c_{pq}^{-+}|p^-\rangle\langle q^+|, \quad (44)$$

where $\epsilon_p^{+(-)}$ and $|p^{+(-)}\rangle$ are eigenstates and eigenfunctions of $H_{\text{spin}}[+(-)\lambda]$ and $c_{pq}^{-+} = \langle p^-|q^+\rangle$ denotes overlap between eigenstates. These eigenvalues, eigenfunctions, and the overlaps are obtained via exact diagonalization (ED) of $H_{\text{spin}}[\pm\lambda]$

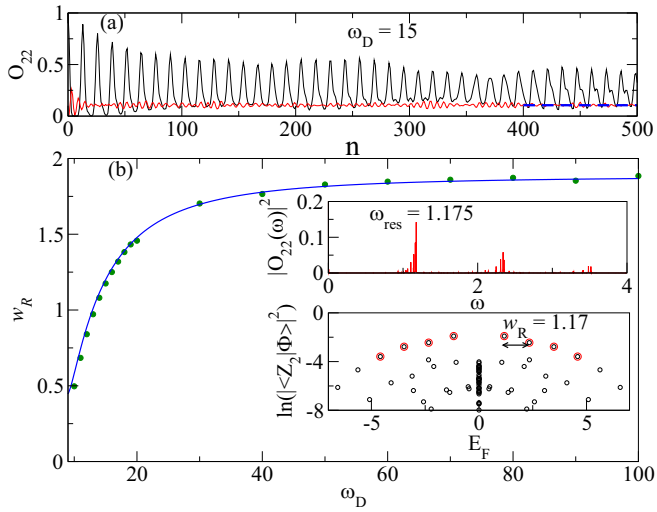

FIG. 1. (a) Plots of O_{22} starting from an initial state $|\mathbb{Z}_2\rangle$ (black solid lines) and $|0\rangle$ (red solid lines), respectively. The blue dashed line indicates the ITE value of O_{22}. (b) Plot of the scar quasienergy separation w_R as a function of ω_D. The green dots show exact numerics while the blue line shows the result of Eq. (38). The top inset shows the Fourier transform of the correlation function $|O_{22}(\omega)|^2$, showing clear peaks at $\omega_{\rm res}$ and its multiples. The bottom inset shows a plot of the overlaps of Floquet eigenstates $|\Phi_n\rangle$ with the initial state ($|\langle\mathbb{Z}_2|\Phi_n\rangle|^2$) as a function of E_F displaying the quasienergy separation (w_R), between the scar states which have maximal overlaps with $|\mathbb{Z}_2\rangle$ (indicated in red). For both insets and for (a) $\omega_D = 15$. All energies (frequencies) are scaled in units of $w/\sqrt{2}$ [$w/(\hbar\sqrt{2})$], $\lambda = 15$ in rescaled units for all plots and $L = 18$ for (a) and $L = 14$ for (b).

for finite system size $L \leqslant 26$. Using these, we compute the spin correlation function,

$$O_{ij} = \langle n_i^r n_{i+j}^r \rangle = \tfrac{1}{4}\langle\psi_0|(U^\dagger)^n\big(1+\sigma_i^z\big)\big(1+\sigma_{i+j}^z\big)U^n|\psi_0\rangle, \quad (45)$$

between any two sites i and $i+j$ is obtained after n drive cycles. Unless explicitly stated otherwise, we will choose the initial state $|\psi_0\rangle = |\mathbb{Z}_2\rangle = |\cdots\downarrow\uparrow\downarrow\uparrow\cdots\rangle$ to be a $\mathbb{Z}_2$ symmetry broken state, with $\langle\psi_0|\sigma_j^z|\psi_0\rangle = (-1)^{j+1}$.

To demonstrate the presence of ergodic to weak ergodicity breaking transitions as a function of the drive frequency ω_D, we compute the dynamics of the correlators starting from $|\mathbb{Z}_2\rangle$. For this, we compute O_{22} from Eq. (45) as a function of the stroboscopic time n (number of drive cycles) for several ω_D. In addition, we also compute the half-chain entanglement entropy $S_{L/2}$ for the eigenstates of the Floquet spectrum. This is carried out by computation of the reduced density matrix for these eigenstates for a half chain from which the half-chain entanglement entropy $S_{L/2}$ can be obtained using a standard procedure. The details of this procedure are outlined in Appendix A. Quantum scars have $S \sim \ln L$ in contrast to thermal states for which $S \sim L$. Thus, $S_{L/2}$ can reliably distinguish between thermal states and scars for finite-size many-body systems.

Let us first consider the regime where $\hbar\omega_D \geqslant \lambda$. The behavior of O_{22} as a function of n is shown in Fig. 1(a). We find that the dynamics exhibits long-time coherent oscillations from an initial $|\mathbb{Z}_2\rangle$ state [black curve in Fig. 1(a), while the dynamics from the Rydberg vacuum state $|0\rangle = |\downarrow\downarrow\downarrow\ldots\rangle$ provides fast thermalization consistent with ETH [red curve in Fig. 1 (a)]. The symmetric nature of $\lambda(t)$ ensures that $\{\prod_{i=1}^L \sigma_i^z, H_F\} = 0$ to all orders in $1/\omega_D$ (where $\{\cdot,\cdot\}$ denotes the anticommutator) (see Appendix B for details); consequently, the spectrum of H_F is symmetric around zero. Since any eigenstate of $\sum_i \sigma_i^z$ (such as $|\psi_0\rangle = |\mathbb{Z}_2\rangle$ or $|0\rangle$) satisfies $\langle\psi_0|H_F|\psi_0\rangle = 0$, this implies that all local correlators should reach their infinite temperature ensemble (ITE) values as per ETH predictions in the absence of scars in the eigenspectrum of H_F. The blue dashed line in the same figure indicates the ITE value of O_{22} which can be calculated analytically as follows.

We first note that the ITE value of O_{22} equals $\mathrm{tr}(O_{22})$ divided by the Hilbert space dimension. Given a system of size L with periodic boundary condition (PBC), and the constraint that two up-spins cannot be on neighboring sites in any state, we can find the number of states by a transfer matrix approach. To this end, we first define the Fibonacci numbers which satisfy $F_n + F_{n+1} = F_{n+2}$, with $F_1 = F_2 = 1$; as n increases, F_n quickly approaches $\varphi^n/\sqrt{5}$, where $\varphi = (\sqrt{5}+1)/2$ is the golden ratio. Keeping the up-spin constraint in mind, we define the transfer matrix

$$A = \begin{pmatrix} 0 & 1 \\ 1 & 1 \end{pmatrix}, \quad (46)$$

where the indices (ij) of A_{ij} can take values 1 (spin-up) and 2 (spin-down). The number of states in an L-site system is then given by $\mathrm{Tr}(A^L) = F_{L-1} + F_{L+1}$. We also need the number of states in an L-site system with open boundary condition (OBC). Since the number of bonds for an OBC system with L sites is $L-1$, the number of states for such a system is given by the sum of all matrix elements of A^{L-1}. This is equal to F_{L+2}. Next, we note that in a given state, O_{22} will be nonzero and equal to 1 only if three consecutive spins, say at sites $(n, n+1, n+2)$, have the configuration $|\uparrow\downarrow\uparrow\rangle$. The constraint of not having two up-spins next to each other implies that the spins at sites $n-1$ and $n+3$ must both be down-spins. The rest of the system consisting of sites $(n+4, n+5, \cdots, L, 1, \cdots, n-3, n-2)$ has OBC, with $L-5$ sites and $L-6$ bonds; the number of states of this subsystem is given by F_{L-3} as shown above. Hence, the infinite temperature ensemble value of $O_{22} = F_{L-3}/(F_{L-1} + F_{L+1})$. As L increases, this rapidly approaches the value $1/(\varphi^2 + \varphi^4) \simeq 0.106$.

While the stroboscopic dynamics of O_{22} in Fig. 1(a) shows similar behavior to the previous studies of quenches in the undriven PXP model, the periodically driven version provides a new drive-induced control over the quasienergy separation of the scars, w_R, and hence on the oscillation frequency which has no analog in earlier quench studies. A plot of w_R for $\hbar\omega_D \geqslant \lambda$ as a function of ω_D is shown in Fig. 1(b). Here w_R is extracted from the quasienergies of the Floquet eigenstates $|\Phi_n\rangle$ that have a large overlap with the $|\mathbb{Z}_2\rangle$ state and simultaneously have anomalously low $S_{L/2}$. The Floquet eigenstates marked in red in the lower inset of Fig. 1(b) satisfy both these properties. The lowering of w_R implies a sharp decrease in the

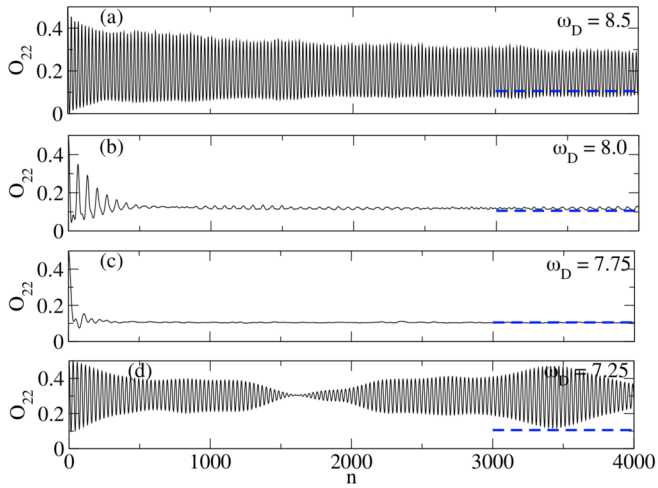

FIG. 2. Plots of O_{22} as a function of n near the transition at the largest drive frequency starting from an initial state $|\psi_0\rangle = (|\mathbb{Z}_2\rangle + |\bar{\mathbb{Z}}_2\rangle)/\sqrt{2}$. The blue dashed line in all panels corresponds to the ITE of O_{22}. Here, $L = 26$ and all units are same as in Fig. 1.

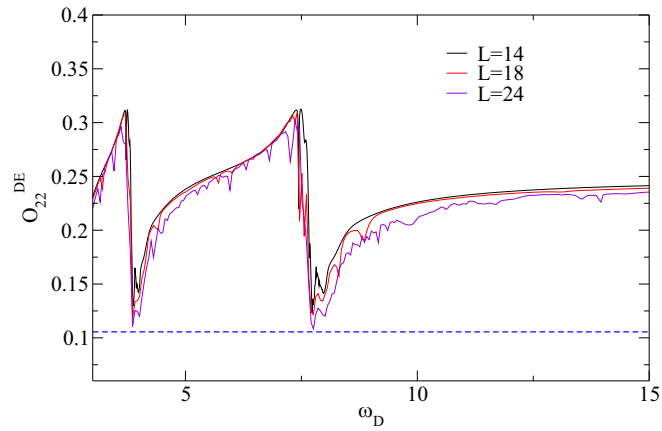

FIG. 3. The behavior of $O_{22}^{\rm DE}$ as a function of ω_D for $|\psi_0\rangle = |\mathbb{Z}_2\rangle$ at sizes $L = 14, 18, 24$. The blue dashed line corresponds to the ITE of O_{22}. All units are same as in Fig. 1.

oscillation frequency $\omega_{\rm res}$ of O_{22} as a function of ω_D in this regime. To check this, we extract $\omega_{\rm res}$ as a function of ω_D from the Fourier transform of O_{22} [upper inset of Fig. 1(b)], which matches the corresponding values of $w_R/\hbar$ almost perfectly [lower inset of Fig. 1(b)]. We note that w_R starts to decrease when $\gamma \to 1$; such a behavior follows from the decrease of the norm of the PXP terms in H_F at $\mathcal{O}(w)$ with increasing γ [Eq. (38)], which gives $w_R = (\sin(\gamma)w_\infty)/\gamma$, where w_∞ is the scar quasienergy separation for the undriven PXP model. Interestingly, the bottom inset of Fig. 1(b) shows a large number of states with zero quasienergy. They arise due to a symmetry of the Floquet operator which is discussed in Appendix B.

Next, we analyze the regime $\hbar\omega_D < \lambda$ where we encounter the reentrant transitions between coherent and thermal regimes. Here, we follow Refs. [15,16] and use the state $|\psi_0\rangle = (|\mathbb{Z}_2\rangle + |\bar{\mathbb{Z}}_2\rangle)/\sqrt{2}$ as our initial state, where $|\bar{\mathbb{Z}}_2\rangle$ denotes the spin-flipped version of $|\mathbb{Z}_2\rangle$. This allows us access to larger L ($L \leqslant 26$) since $|\psi_0\rangle$ has weight only in the sector with zero total momentum and spatial inversion (parity) symmetry.

The result of evolution of O_{22} in this subspace is shown in Fig. 2 near the first reentrant transition for a large number of drive cycles $n \leqslant 4000$. Figure 2(a) shows weak ergodicity breaking persistent oscillatory dynamics at $\omega_D = 8.5$. As we reduce ω_D, these oscillations dampen [Fig. 2(b)]; such a behavior can be interpreted as a precursor to ergodic dynamics and thermalization. Upon further reduction of ω_D, ergodic dynamics consistent with ETH sets in and the fastest thermalization is seen around $\omega_D = 7.75$ [Fig. 2(c)]. Finally, at lower ω_D, the persistent oscillations return [Fig. 2(d)]. The non-PXP terms present in the Floquet Hamiltonian [Eq. (39)] also lead to a distinct beating pattern in the oscillations in O_{22} at $\omega_D = 7.25$ [Fig. 2(d)], which is absent in the oscillations at a higher drive frequency $\omega_D = 8.5$ [Fig. 2(a)].

In the $n \to \infty$ limit, the system can be locally described by the diagonal ensemble [37] since the rapidly oscillating terms in Eq. (47) below can be dropped when $n \gg 1$,

$$\begin{aligned}\langle\psi_0|(U^\dagger)^n O_{22} U^n|\psi_0\rangle &= \sum_i |c_i|^2 \langle\Phi_i|O_{22}|\Phi_i\rangle \\ &+ \sum_{i\neq j} \langle\psi_0|\Phi_j\rangle\langle\Phi_i|\psi_0\rangle\langle\Phi_j|O_{22}|\Phi_i\rangle e^{-inT(E_{Fi}-E_{Fj})}, \quad (47)\end{aligned}$$

where $U|\Phi_i\rangle = e^{-iE_{Fi}T}|\Phi_i\rangle$ and $|c_i|^2 = |\langle\Phi_i|\psi_0\rangle|^2$. This gives the diagonal ensemble value for O_{22} to be

$$O_{22}^{\rm DE} = \sum_i |c_i|^2 \langle\Phi_i|O_{22}|\Phi_i\rangle. \quad (48)$$

We show the behavior of $O_{22}^{\rm DE}$ as a function of ω_D for $|\psi_0\rangle = |\mathbb{Z}_2\rangle$ in Fig. 3 for $L = 14, 18$ and 24. Figure 3 clearly shows the sharp decrease in $O_{22}^{\rm DE}$ toward the ITE value in the neighborhood of drive frequencies with the fastest thermalization and its tendency to saturate to much higher non-ITE values when ω_D is sufficiently away from these frequencies.

Such transitions can be tied to the presence or absence of Floquet scars in the spectrum of H_F. This is shown in Fig. 4. Figure 4(a) ($\omega_D = 8.5$) and Fig. 4(d) ($\omega_D = 7.25$) clearly indicate the presence of scars having high overlap with $(|\mathbb{Z}_2\rangle + |\bar{\mathbb{Z}}_2\rangle)/\sqrt{2}$. This is consistent with the presence of weak ergodicity breaking dynamics characterized by persistent long-time oscillations [Figs. 2(a) and 2(d)]. These scar states start to merge with the thermal band around $\omega_D = 8.0$ [Fig. 4(b)], indicating precursor to the thermal behavior [Fig. 2(b)]. Figure 4(c) at $\omega_D = 7.75$ shows complete absence of scars resulting in ergodic dynamics of O_{22} and fast thermalization predicted by ETH [Fig. 2(c)].

The behavior of the fidelity of the state after n drive cycles, which serves as another indicator of the transition, is defined as

$$\mathcal{F}(n) = |\langle\Psi(n)|\Psi_0\rangle|^2, \quad (49)$$

where $|\Psi(n)\rangle$ denotes the state of the system after n cycles of the drive, and $|\psi_0\rangle$ is the initial state. In the regime where the dynamics is dominated by scars, the presence of long-term coherent oscillations indicates that one could expect

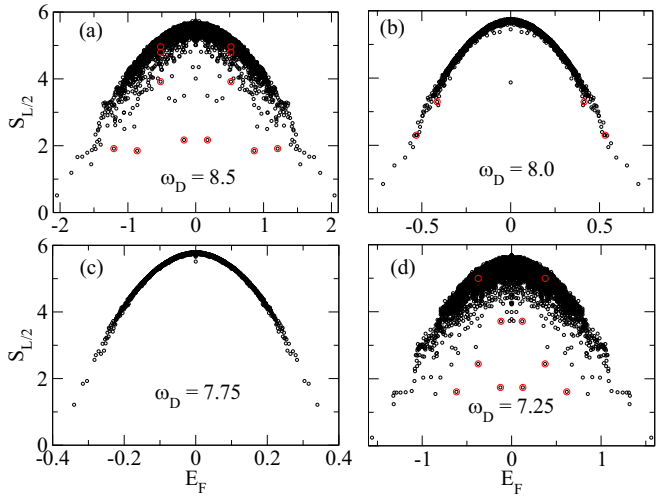

FIG. 4. Plots of $S_{L/2}$ near the transition at the largest drive frequency showing the presence and absence of scars in the Floquet eigenspectrum. States that have high overlaps with the initial state ($|\langle\psi_0|\Phi_n\rangle|^2 \geqslant 10^{-2}$) are marked in red. All other parameters are same as in Fig. 2.

periodic revival of $\mathcal{F}(n)$ to values near unity; in contrast, the thermal region, $\mathcal{F}(n)$ is expected to decay rapidly to zero and never revive. These behaviors are numerically confirmed in Fig. 5 near the ergodic to weak ergodicity breaking transition around $\omega_D = 7.75$. The top left ($\omega_D = 8.5$) and the bottom right ($\omega_D = 7.25$) panels display periodic persistent revivals of $\mathcal{F}(n)$ before and after the first transition. Such revivals are completely absent in the bottom left panel ($\omega_D = 7.75$) in the thermal region where $\mathcal{F}(n)$ decays to zero without any subsequent revival. The top right panel ($\omega_D = 8$) shows an intermediate behavior displaying a few (smaller) revivals and subsequent decay. This indicates a crossover from a coherent

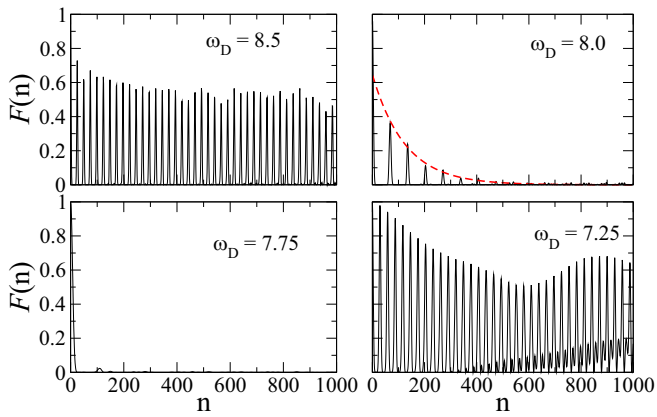

FIG. 5. Plot of the fidelity $\mathcal{F}(n)$ as a function of n showing periodic persistent revivals where the dynamics is controlled by scars [top left and bottom right panels] and fast decay with no subsequent revival in their absence [bottom left panel]. An intermediate behavior indicating crossover from coherent to thermal regime is shown in the top right panel. The top right panel also shows a fit to $\exp(-n/\tau)$ (dotted red curve) to extract the relaxation timescale, τ, to ETH. All other parameters are same as in Fig. 2.

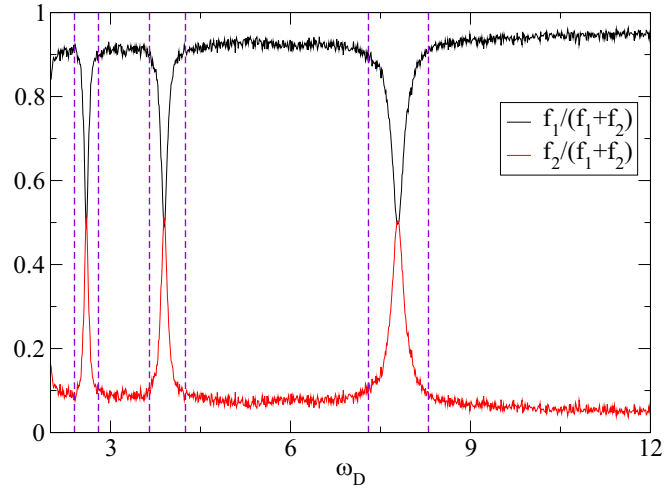

FIG. 6. Plots of $f_1/(f_1 + f_2)$ (in black) and $f_2/(f_1 + f_2)$ (in red) as a function of the drive frequency ω_D calculated for $\lambda = 15$ in rescaled units and $L = 14$. The ergodic regimes are indicated by dashed vertical lines. All units are same as in Fig. 1.

to a thermal regime. In the regime where $\mathcal{F}(n)$ shows no revivals, its decay is fitted to a form $\exp(-n/\tau)$ (top right panel of Fig. 5) to extract the relaxation timescale τ to ETH as shown in the inset of Fig. 7.

The mechanism of these transitions is rather transparent in the large amplitude regime ($\lambda \gg w$). Unless the drive frequency ω_D is near one of the special frequencies $\hbar\omega_D = \lambda/(2n_0)$ where n_0 is a positive integer, the $\mathcal{O}(w)$ terms in the Floquet Hamiltonian [Eq. (38)] dominates over the non-PXP terms [Eq. (39)] that occur at $\mathcal{O}(w^3)$ and higher. Then the

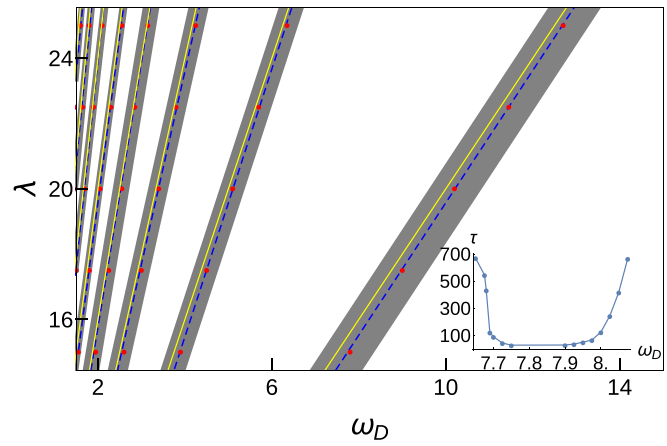

FIG. 7. Schematic phase diagram showing reentrant transitions between ergodic and weak ergodicity breaking regimes as a function of ω_D and λ. The red dots joined by dashed blue lines indicate locations of $\omega_D = \omega_D^c$ where O_{22} displays fastest thermalization, while the gray-shaded regions indicate range of ω_D around ω_D^c for which it shows a precursor to thermalization. The yellow solid lines indicate the positions of the transition obtained analytically from Eq. (38). The white regions are where O_{22} shows long-time persistent oscillations. All energies (frequencies) are scaled in units of $w/\sqrt{2}$ [$w/(\hbar\sqrt{2})$]. The inset shows the relaxation timescale (τ) to ETH in the vicinity of the first reentrant transition.

Floquet Hamiltonian H_F is very well approximated by a renormalized PXP model [Eq. (38)] and thus hosts Floquet scars which results in coherent oscillations starting from the $|\mathbb{Z}_2\rangle$ state. In contrast, near $\hbar\omega_D = \lambda/(2n_0)$, the $\mathcal{O}(w)$ contribution to H_F is suppressed and the contributions from the non-PXP terms at $\mathcal{O}(w^3)$ become important. In the presence of such non-PXP terms which can be long-ranged at low ω_D, H_F does not support scars and hence the dynamics starting from the $|\mathbb{Z}_2\rangle$ state does not show weak ergodicity breaking coherent oscillations and instead thermalizes. The competition between the PXP and the non-PXP terms in H_F which can be controlled by w/λ at any ω_D is thus crucial for generating these two dynamical regimes.

To numerically estimate the relative importance of the PXP and the non-PXP terms, we compute the norm of the (non-) PXP-like terms in the Floquet Hamiltonian numerically using $L = 14$. To this end, we write the matrix representation of H_F in the basis states $|\phi_n\rangle$ of σ^z and identify the matrix elements that have $\langle\phi_n|\sum_\ell \tilde{\sigma}_\ell^{x/y}|\phi_m\rangle \neq 0$. Let us denote this set as $\mathcal{N}_0$ which has $N_0 = 2LF_{L-1}$ elements. We then define f_1 and f_2 as

$$f_{1[2]} = \frac{1}{N_0} \sum_{\{n,m\}\in[\notin]\mathcal{N}_0} |\langle\phi_n|H_F|\phi_m\rangle|^2. \tag{50}$$

Clearly, f_2 represents the contribution from the non-PXP type of terms in H_F. We note that in general f_1 will also have contributions from non-PXP terms since such terms may have nonzero matrix elements for some states included in $\mathcal{N}_0$. However, at large λ/w, the contributions from these terms are expected to be small by at least $\mathcal{O}(w^2/\lambda^2)$. The behavior of $f_1/(f_1+f_2)$ and $f_2/(f_1+f_2)$ as a function of ω_D (Fig. 6) clearly shows that $f_1 \gg f_2$ in the coherent (weak ergodicity breaking) regime while f_2 starts approaching f_1 in the thermal (ergodic) regime.

The schematic phase diagram for these reentrant ergodic to weak ergodicity breaking transitions is summarized in Fig. 7. The ergodic regions, where O_{22} displays either complete ergodic behavior or a precursor to thermalization, are located in a small frequency window (shown schematically in gray whose width is indicated in Fig. 6) around ω_D^c (indicated as red dots joined by blue dashed lines in Fig. 7), where ω_D^c denotes the frequency at which O_{22} shows the fastest approach to its ETH value and is determined numerically ($f_1 \approx f_2$ at such drive frequencies as can be seen in Fig. 6). The inset of Fig. 7 shows the relaxation timescale to ETH (denoted by τ) around ω_D^c near the first reentrant transition which rapidly increases by at least three orders of magnitude within the ergodic regime as the coherent regime is approached from either side of ω_D^c. The yellow lines indicate the positions of the transitions as obtained from Eq. (38) (i.e., $\lambda/(\hbar\omega_D) = 2n_0$), while the white regions denote the ranges of ω_D where O_{22} shows weak ergodicity breaking oscillatory dynamics. The thermal regions become denser with decreasing ω_D and ultimately merge into a continuum where weak ergodicity breaking coherent dynamics of O_{22} ceases to exist.

IV. DISCUSSION

In this work we have studied the kinematically constrained PXP model, a paradigmatic model for ETH violating quantum scars, in the presence of a pulsed transverse magnetic field that varies periodically in time. This model serves as the effective low-energy model for experimentally realized Rydberg atoms. We have used numerical techniques such as ED to study the dynamics of this model. In addition, we have used a novel perturbative approach at large drive amplitude to derive a Floquet Hamiltonian for the system which provides analytic, albeit qualitative, understanding of its properties at both high and low frequency regime. Moreover, the Floquet Hamiltonian which we have derived constitutes a resummation of all terms of its Magnus counterpart in the high drive amplitude limit.

Our study reveals that the correlator dynamics in this model starting from an initial $|\mathbb{Z}_2\rangle$ state and in the presence of a periodic drive hosts persistent oscillations for a wide range of parameter values. The presence of these oscillations can be attributed to quantum scars in the Floquet Hamiltonian of such a model which has high overlap with the initial states. These scars, in contrast to their counterparts in the PXP model studied earlier, are present for arbitrary values of λ as long as $\lambda/(\hbar\omega_D) \leqslant 1$. In this regime, the energy separation of these scars control the frequency of the correlator oscillations. These energy separations can be tuned by changing the drive frequency and this effect can be understood within the Magnus expansion yielding a renormalized PXP model for the Floquet Hamiltonian for $\lambda/\omega_D \leqslant 1$.

In contrast for $\lambda/(\hbar\omega_D) > 1$ and $\lambda/w \gg 1$, our study finds several reentrant transitions as a function of drive frequencies from regimes with scars to those without them. In the latter regime, persistent oscillations are absent; instead, the system shows fast thermalization consistent with ETH. The reentrant nature of these transitions can be qualitatively understood from the Floquet Hamiltonian [Eqs. (38) and (39)]. We find that there are certain special frequencies at which the norm of the $\mathcal{O}(w)$ Floquet Hamiltonian, which is of the PXP form, vanishes. In the vicinity of these points, the dynamics is controlled by non-PXP [$\mathcal{O}(w^3)$] terms in the Floquet Hamiltonian which do not support scars. For these drive frequency ranges, the systems therefore shows ergodic behavior consistent with ETH. As we move away from these frequencies to regime where the norm of the $\mathcal{O}(w)$ term is large, the dynamics is again scar dominated leading to persistent oscillation, weak ergodicity breaking behavior, and violation of ETH. These reentrant transitions from weak ergodicity breaking to ergodic regimes produced by tuning the drive frequency are possibly the first example of this kind in a quantum many-body system without any spatial disorder.

The fate of these transitions in the thermodynamic limit remains unclear and is left as a subject of future study. We conjecture, however, that these transition will disappear in the thermodynamics limit since the overlap of $|\mathbb{Z}_2\rangle$ with scar states turns out to be an exponentially decreasing function of L. Consequently, one expects the effect of scars on the dynamics at large L to be small and ETH to take over. However, for the system sizes we could numerically access in our studies, this regime is never reached. Furthermore, it is to be noted that the presence of scars in the thermodynamic limit in the tilted Bose-Hubbard or the PXP model itself is an unanswered question. In this context, we would like to point out that the presence of scars like states in the thermodynamics limit has been analytically shown for AKLT chains [21].

Our results can be easily verified by standard experiments using finite-size Rydberg chains [12]. Here we predict that a periodic variation of the chemical potential Δ for the Rydberg atoms with a fixed frequency ω_D and large amplitude $\Delta_0 \gg \Omega$ should yield dynamics with persistent oscillation of the correlation function $\langle n^r_\ell n^r_{\ell+2}\rangle$ for any fixed ℓ provided $\Delta_0/(\hbar\omega_D) \leqslant 1$. At higher value of $\Delta_0/(\hbar\omega_D)$, we predict a transition to thermal behavior for the correlator followed by a reentrance to the persistent oscillation regime. This would constitute an experimental signature of collapse and revival of scar states for Rydberg chains.

In conclusion, we have studied the periodic dynamics of the driven dipole or equivalently the constrained PXP model. Our study leads to an analytic $\mathcal{O}(w)$ Floquet Hamiltonian in the high drive amplitude limit, demonstrates the presence of scars in the exact Floquet spectrum of the system, shows the possibility of Floquet engineering of their energy spacings controlling the oscillatory dynamics of the density-density correlation function, and unravels the presence of a reentrant, coherent oscillatory to incoherent thermal transition as a function of drive frequency for large drive amplitude. We also suggest experiments which can test our theory.

ACKNOWLEDGMENTS

The work of A.S. is partly supported through the Max Planck Partner Group program between the Indian Association for the Cultivation of Science (Kolkata) and the Max Planck Institute for the Physics of Complex Systems (Dresden). D.S. thanks DST, India for financial support through Project No. SR/S2/JCB-44/2010.

APPENDIX A: HALF-CHAIN ENTANGLEMENT

In this Appendix we detail out the procedure for computation of the half-chain entanglement $S_{L/2}$ used in the main text. The procedure could be applied to equilibrium or Floquet eigenstates or to an arbitrary driven state of the given model in Eq. (6).

We first note that the full density matrix (DM) is given by $\rho_{AB} = |\psi\rangle\langle\psi|$ where AB is the whole system of size L with PBC. We divide this system into two parts A and B of size $L/2$ each with OBC as schematically shown in Fig. 8.

Next, we calculate the reduced density matrix of any of the subsystems by integrating out the other subsystem. This leads to

$$\rho_{A(B)} = Tr_{B(A)}\rho_{AB}. \tag{A1}$$

This procedure involves taking a partial trace over the environment degrees of freedom. For example, the (ij)th element, $\rho_A(i, j)$, of the reduced density matrix is given by

$$\rho_A(ij) = \sum_{k=1}^{\mathrm{HSD}_B^{\mathrm{OBC}}} \langle i;k|\rho_{AB}|k;j\rangle, \tag{A2}$$

where i and j represent product states in A, and k represent product states in B with OBC. However, since the full system (AB) had PBC, the Hilbert space dimension (HSD) of AB does not match the HSD of $\mathcal{H}_A \otimes \mathcal{H}_B$ with OBC. To see this, we note that $\mathrm{HSD}_L^{PBC} = F_{L-1} + F_{L+1}$ and $\mathrm{HSD}_L^{\mathrm{OBC}} = F_{L+2}$,

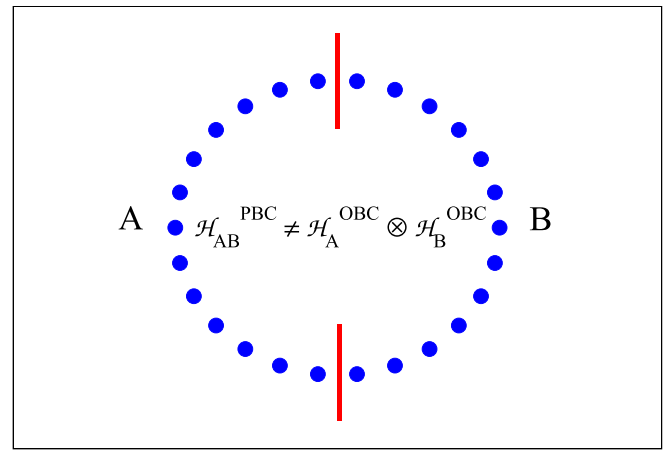

FIG. 8. Schematic representation of the bipartition of the one-dimensional model considered here [Eq. (6)] with periodic boundary condition.

where F_L denotes the Lth Fibonacci number. Since $F_{L+2} = F_L + F_{L+1} > F_{L-1} + F_{L+1}$ for any L, one has $F_{L_1+2}F_{L_2+2} > F_{L_1+L_2-1} + F_{L_1+L_2+1}$ for any L_1, L_2. Thus, while taking the summation in Eq. (A1), one has to exclude the states for which at any one of the junctions marked in red in Fig. 8, the end points of both A and B are occupied by a dipole.

Since the Hamiltonian and hence the full density matrix is in the configuration (product) basis, any matrix element of the reduced density matrix can be expressed as a sum of some of the elements of full DM, and we can rewrite Eq. (A2) as

$$\rho_A(ij) = \sum_{k=1}^{\mathrm{HSD}_B^{\mathrm{OBC}}} \rho_{AB}(i;k,k;j). \tag{A3}$$

We stress here that one needs to be careful about this procedure if the density matrix is expressed using some other basis. For example, in our case $\rho_{AB} = \sum_{m,n} \rho(m,n)|m\rangle\langle n|$ where $|m\rangle$, $|n\rangle$ are states in the zero total momentum $(K = 0)$ and even parity $(P = +1)$ sector. In this case,

$$\rho_A(ij) = \sum_{k=1}^{\mathrm{HSD}_B^{\mathrm{OBC}}} \langle i;k|\,(\sum_{m,n}\rho(m,n)|m\rangle\langle n|)\,|k;j\rangle. \tag{A4}$$

This indicates that one needs to search for states $|m^{i;k}\rangle$, $|n^{j;k}\rangle$ having nonzero overlap with the states $|i;k\rangle$ and $|j;k\rangle$ given by

$$|m^{i;k}\rangle = \frac{1}{\sqrt{L_m^{i;k}}}(\cdots + |i;k\rangle + \cdots),$$
$$|n^{j;k}\rangle = \frac{1}{\sqrt{L_n^{j;k}}}(\cdots + |j;k\rangle + \cdots). \tag{A5}$$

In this case, (i, j)th element of ρ_A is given by

$$\rho_A(ij) = \sum_{k=1}^{\mathrm{HSD}_B^{\mathrm{OBC}}} \frac{1}{\sqrt{L_m^{i;k}L_n^{j;k}}}\rho_{AB}(m^{i;k}, n^{j;k}), \tag{A6}$$

and the diagonalization of ρ_A gives the von Neumann entropy since $S_A = -\sum_{i=1}^{\mathrm{HSD}_A^{\mathrm{OBC}}} p_i \ln(p_i)$, where p_i are the eigenvalues of ρ_A. This procedure is used to compute $S_{L/2}$ in the main text.

APPENDIX B: SYMMETRY OF FLOQUET OPERATOR AND ZERO MODES

We will now discuss an exact symmetry of the Floquet operator for our driving protocal. We will then see that this symmetry implies that there will be a large number of states with zero quasienergy.

We define an operator

$$Q = \prod_{n=1}^{L} \sigma_n^z, \tag{B1}$$

which is unitary and satisfies $Q^{-1} = Q$. The eigenvalues of Q are ± 1, and the corresponding eigenstates have an even (odd) number of down spins. Next, we see that Q anticommutes with the first term and commutes with the second term in Eq. (6). As a result, the Floquet operator defined in Eq. (7) satisfies

$$U^{-1} = QUQ. \tag{B2}$$

This means that if $|\psi_n\rangle$ is an eigenstate of U with eigenvalue $e^{-i\theta_n}$, $Q|\psi_n\rangle$ will be an eigenstate of U with eigenvalue $e^{i\theta_n}$. Hence, all the quasienergies must come in $\pm$ pairs, except for quasienergies 0 and π which correspond to Floquet eigenvalues equal to ± 1. We also see that eigenstates of U with eigenvalues ± 1 can be simultaneously chosen to be eigenstates of Q; hence they will be superpositions of states all of which have an even or an odd number of down spins.

Given the Floquet Hamiltonian H_F defined through $U = e^{-iH_F T/\hbar}$, Eq. (B2) implies that

$$QH_F Q = -H_F. \tag{B3}$$

Note that this is an exact symmetry, independent of the Magnus expansion or Floquet perturbation theory. We will now use the arguments given in Ref. [15] to argue that there will be a large number of eigenstates of H_F with zero eigenvalue; we will call these zero modes. Equation (B3) implies that H_F can be thought of as defining a tight-binding model of a particle moving on a bipartite lattice, where the two sublattices correspond to eigenvalues of Q being equal to ± 1. For such a tight-binding model, it is known that a lower bound on the number of zero modes is given by the difference of the number of states with Q equal to ± 1.

Next, we use the parity symmetry of our system corresponding to a reflection about the middle of the bond connecting sites labeled $L/2$ and $L/2+1$ (we will assume that L is even). We define a parity transformation P which does this reflection. Given an arbitrary state $|\psi\rangle$, the parity transformed state is $P|\psi\rangle$. The superpositions $|\psi\rangle \pm P|\psi\rangle$ then give two states with even (odd) parity, respectively. However, states of the product form

$$|\psi\rangle = |\sigma_1\sigma_2\cdots\sigma_{L/2-1}\sigma_{L/2}\sigma_{L/2}\sigma_{L/2-1}\cdots\sigma_2\sigma_1\rangle, \tag{B4}$$

where each σ_n can be spin-up or down, clearly satisfy $P|\psi\rangle = |\psi\rangle$. Such states therefore lie in the even parity sector; further, they have eigenvalue of Q equal to $+1$ since each value of σ_i appears twice in Eq. (B4). Let the number of such states be N' (we will calculate this number below). Now, let N_{PQ} denote the number of orthonormal states with $P = \pm$ (denoting even/odd) and $Q = \pm$ (denoting ± 1). We then see that $N_{++} = N_{-+} + N'$ and $N_{+-} = N_{--}$. A lower bound on the number of zero modes in the odd parity sector is $|N_{-+} - N_{--}|$, and in the even parity sector is $|N_{++} - N_{+-}| = |N_{-+} - N_{--} + N'|$. Since

$$|N_{-+} - N_{--} + N'| + |N_{-+} - N_{--}| \geqslant N', \tag{B5}$$

regardless of the values of N_{-+} and N_{--}, we see that N' gives a lower bound on the number of zero modes.

To calculate the number N', we note that the string $(\sigma_1, \sigma_2, \cdots, \sigma_{L/2})$ for the first $L/2$ sites in Eq. (B4) must begin and end with a down spin to ensure that the neighboring sites $(L/2, L/2+1)$ and $(L, 1)$ do not both have spin-up. The number of of such strings is given by the 22 matrix element of $A^{L/2-1}$; this gives $N' = F_{L/2}$. Thus, the number of zero modes increases exponentially with L, as $\varphi^{L/2}/\sqrt{5}$.

[1] J. Dziarmaga, Adv. Phys. **59**, 1063 (2010).
[2] A. Polkovnikov, K. Sengupta, A. Silva, and M. Vengalattore, Rev. Mod. Phys. **83**, 863 (2011).
[3] A. Dutta, G. Aeppli, B. K. Chakrabarti, U. Divakaran, T. F. Rosenbaum, and D. Sen, *Quantum Phase Transitions in Transverse Field Spin Models: From Statistical Physics to Quantum Information* (Cambridge University Press, Cambridge, 2015).
[4] S. Mondal, D. Sen, and K. Sengupta, *Quantum Quenching, Annealing and Computation*, edited by A. Das, A. Chandra, and B. K. Chakrabarti, Lecture Notes in Physics Vol. 802 (Springer, Berlin/Heidelberg, 2010), Chap. 2, p. 21.
[5] L. D'Alessio, Y. Kafri, A. Polkovnikov, and M. Rigol, Adv. Phys. **65**, 239 (2016).
[6] J. M. Deutsch, Phys. Rev. A **43**, 2046 (1991).
[7] M. Srednicki, Phys. Rev. E **50**, 888 (1994); J. Phys. A **32**, 1163 (1999).
[8] M. Rigol, V. Dunjko, and M. Olshanii, Nature (London) **452**, 854 (2008).
[9] M. Basko, I. L. Aleiner, and B. L. Altshuler, Ann. Phys. **321**, 1126 (2006).
[10] R. Nandkishore and D. Huse, Ann. Rev. Cond. Mat. **6**, 15 (2015).
[11] E. J. Heller, Phys. Rev. Lett. **53**, 1515 (1984).
[12] H. Bernien *et al.*, Nature **551**, 579 (2017).
[13] S. Choi, C. J. Turner, H. Pichler, W. W. Ho, A. A. Michailidis, Z. Papić, M. Serbyn, M. D. Lukin, and D. A. Abanin, Phys. Rev. Lett. **122**, 220603 (2019).
[14] W. W. Ho, S. Choi, H. Pichler, and M. D. Lukin, Phys. Rev. Lett. **122**, 040603 (2019).
[15] C. J. Turner, A. A. Michailidis, D. A. Abanin, M. Serbyn, and Z. Papić, Nat. Phys. **14**, 745 (2018).
[16] C. J. Turner, A. A. Michailidis, D. A. Abanin, M. Serbyn, and Z. Papić, Phys. Rev. B **98**, 155134 (2018).

[17] K. Bull, I. Martin, and Z. Papić, Phys. Rev. Lett. **123**, 030601 (2019).
[18] V. Khemani, C. R. Laumann, and A. Chandran, Phys. Rev. B **99**, 161101(R) (2019).
[19] S. Moudgalya, N. Regnault, and B. A. Bernevig, Phys. Rev. B **98**, 235156 (2018).
[20] T. Iadecola, M. Schecter, and S. Xu, Phys. Rev. B **100**, 184312 (2019).
[21] N. Shiraishi, J. Stat. Mech. (2019) 083103.
[22] M. Schecter and T. Iadecola, Phys. Rev. Lett. **123**, 147201 (2019).
[23] M. Bukov, L. D'Alessio, and A. Polkovnikov, Adv. Phys. **64**, 139 (2015).
[24] A. Lazarides, A. Das, and R. Moessner, Phys. Rev. E **90**, 012110 (2014).
[25] P. Ponte, A. Chandran, Z.Papić, and D. A. Abanin, Ann. Phys. **353**, 196 (2014).
[26] L. D'Alessio and M. Rigol, Phys. Rev. X **4**, 041048 (2014).
[27] R. Moessner and S. L. Sondhi, Nat. Phys. **13**, 424 (2017).
[28] P. Fendley, K. Sengupta, and S. Sachdev, Phys. Rev. B **69**, 075106 (2004).
[29] R. Samajdar, S. Choi, H. Pichler, M. D. Lukin, and S. Sachdev, Phys. Rev. A **98**, 023614 (2018).
[30] R. Ghosh, A. Sen, and K. Sengupta, Phys. Rev. B **97**, 014309 (2018).
[31] S. Sachdev, K. Sengupta, and S. M. Girvin, Phys. Rev. B **66**, 075128 (2002).
[32] S. Pielawa, T. Kitagawa, E. Berg, and S. Sachdev, Phys. Rev. B **83**, 205135 (2011).
[33] J. Simon, W. S. Bakr, R. Ma, M. E. Tai, P. M. Preiss, and M. Greiner, Nature (London) **472**, 307 (2011); W. Bakr, A. Peng, E. Tai, R. Ma, J. Simon, J. Gillen, S. Foelling, L. Pollet, and M. Greiner, Science **329**, 547 (2010).
[34] K. Sengupta, S. Powell, and S. Sachdev, Phys. Rev. A **69**, 053616 (2004); M. Kolodrubetz, D. Pekker, B. K. Clark, and K. Sengupta, Phys. Rev. B **85**, 100505(R) (2012); U. Divakaran and K. Sengupta, *ibid.* **90**, 184303 (2014).
[35] A. Soori and D. Sen, Phys. Rev. B **82**, 115432 (2010).
[36] T. Bilitewski and N. R. Cooper, Phys. Rev A **91**, 063611 (2015).
[37] P. Reimann, Phys. Rev. Lett. **101**, 190403 (2008).